

## Scanning tunneling spectroscopy under pulsed spin injection

J. Ngai, Y. C. Tseng,<sup>a)</sup> P. Morales, V. Pribiag,<sup>c)</sup> and J. Y. T. Wei<sup>b)</sup>  
*Department of Physics, University of Toronto, 60 St. George Street, Toronto, Ontario M5S1A7 Canada*

F. Chen and D. D. Perovic  
*Department of Materials Science and Engineering, University of Toronto, 184 College Street, Toronto, Ontario M5S3E4 Canada*

(Received 10 October 2003; accepted 13 January 2004)

An experimental technique combining cryogenic scanning tunneling spectroscopy (STS) and pulsed quasiparticle spin injection has been developed. The spin injection is intended to perturb a superconducting thin film from spin equilibrium, while the STS monitors its steady-state quasiparticle spectrum. A pulsed injection circuit was designed to minimize Joule heating while being both synchronized with and decoupled from the STS circuitry. A detailed description of the technique is presented, along with its application to spin-injection heterostructures comprising the half-metallic ferromagnet  $\text{La}_{0.7}\text{Ca}_{0.3}\text{MnO}_3$  and the high- $T_c$  superconductor  $\text{YBa}_2\text{Cu}_3\text{O}_{7-\delta}$ .  
 © 2004 American Institute of Physics. [DOI: 10.1063/1.1667281]

Fundamental processes in strongly correlated electronic materials tend to occur at the nanometer length scales and depend intimately on spin. Cryogenic scanning tunneling spectroscopy (STS), with its extremely fine spatial (<nm) and energy (<meV) resolutions, has proven to be a powerful nanoscale probe of the electronic structures of such materials.<sup>1,2</sup> Recent advances in nanofabrication techniques have also enabled many of these materials to be studied under spin injection.<sup>3</sup> Generically speaking, spin injection is a technique for introducing steady-state spin disequilibrium into such materials to alter their underlying electronic correlations. In a high- $T_c$  superconducting (HTS) thin film, for example, the injection of spin-polarized quasiparticles could suppress the superconductivity by breaking the spin-neutral Cooper pairs.<sup>4,5</sup> Detailed knowledge of how the pair potential responds to such spin perturbations, especially at the coherence-length scales, would thus yield important information on the pairing mechanism.

In this work, we present an experimental technique combining cryogenic STS and pulsed spin injection. At the center of this technique is a STS-compatible *pulsed* current-injection circuit that reduces Joule heating of the sample due to the injection. Also essential are the geometry and dimensions of the spin-injection sample structure, which was designed to avoid transfer-length and spin-diffusion limitations.<sup>6</sup> We demonstrate the feasibility of this technique, by applying it to spin-injection heterostructures comprising thin films of the HTS cuprate and the half-metallic manganite. We discuss the physical significance of our results for the understanding of HTS, and general implications of our technique for the study of electronic materials.

In a conventional STS circuitry, current versus voltage STS is performed by momentarily suspending the feedback loop to hold the tip over a fixed spot on the sample, then

measuring the tunneling current,  $I$ , as a function of the voltage,  $V$ , biasing the tip relative to the sample.<sup>7</sup> The  $V$  bias is typically swept through a series of steps, and the  $I$  data are acquired during a short time window within each  $V$  step.

In our STS circuitry, which can perform spectroscopy on a sample under *pulsed* spin injection, the injection current source must be synchronized with this data-acquisition window [Fig. 2(b)]. The purpose for the triggered short pulse ( $\sim 200 \mu\text{s}$ ) is to reduce any Joule heating due to the injection current. This pulsed current source must also be made to “float” with respect to the STS ground [Fig. 1(a)], in order to avoid any interference with either the bias voltage or the STS feedback circuit.

Figure 2(a) shows a schematic of the pulsed-current circuit. Batteries provide the source for a low-noise “floating” current, while an optocoupler serves to decouple the triggering by the “external” scanning tunneling microscope electronics from the “internal” injection electronics of this circuit. The optocoupler acts as an ideal switch controlled only by the amount of current running through the photodiode located inside. The switch is only turned “on” when a current is running through the photodiode. A voltage pulse from an external function generator, which is TTL triggered by the STS bias-voltage steps, creates a current pulse through the resistor R1 and the photodiode of the optocoupler. The current running through the photodiode “turns on” the optocoupler that acts as a shorting switch between the gate and the drain of a power metal-oxide-semiconductor field effect transistor (MOSFET). With the gate and drain of the MOSFET shorted, a current will flow through the circuit and in through the sample load. A variable serial resistor ( $R_{\text{variable}}$ ) is used within the circuit to vary the amplitude of the pulsed current. The pulsed current running through the circuit and sample is measured by monitoring the voltage drop over a serial resistor ( $R_{\text{monitor}}$ ) at the low side of the circuit. Typical values for the various resistors are indicated in the caption of Fig. 2(a) along with the resultant current levels achieved. The values of the various components can be ad-

<sup>a)</sup>Current address: Department of Electrical Engineering, University of California Berkeley, Berkeley, CA 94720.

<sup>b)</sup>Electronic mail: wei@physics.utoronto.ca

<sup>c)</sup>Current address: Cornell University, 109 Clark Hall, Ithaca, NY 14853-2501.

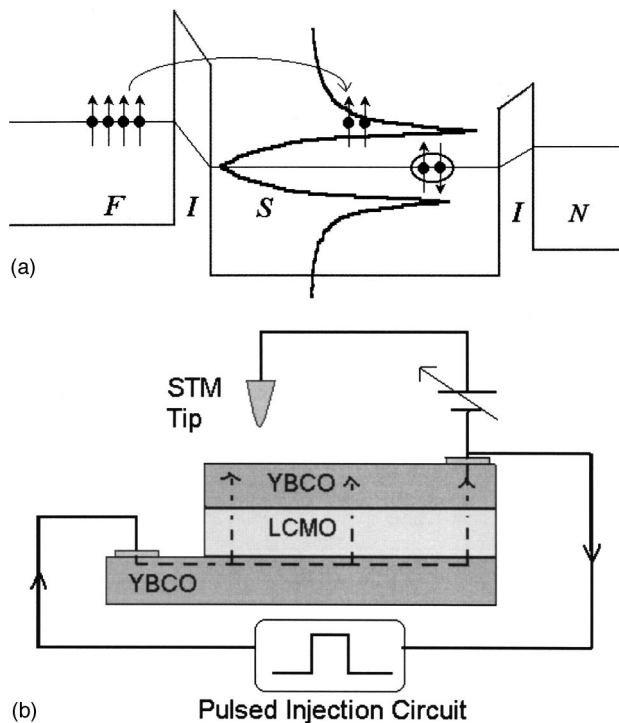


FIG. 1. (a) Schematic of physical processes occurring in our experiments. Left-hand side shows spin polarized quasiparticles tunneling from ferromagnetic LCMO (F) layer into the quasiparticle spectrum of the superconducting YBCO (S) layer while tunneling spectroscopy occurs on the right-hand side from a normal metal tip (N). (b) Schematic of experimental geometry. Spin-injection circuit sends pulsed current through trilayer sample while STS measurements occur simultaneously above.

justed according to experimental conditions and the material systems being examined.

Figure 2(b) shows the voltage-bias, pulsed-injection, and data-acquisition timing scheme. The voltage steps (T0)

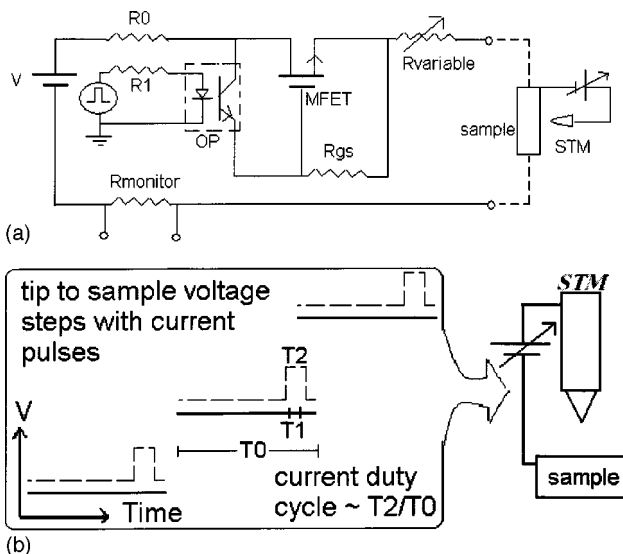


FIG. 2. (a) Schematic of pulsed injection circuitry. Small dashed box labeled OP represents the optocoupler acting as a switch to short the gate and drain of the MOSFET (labeled MFET). Typical values of labeled components are as follows:  $V=18$  V;  $R_0=10$   $\Omega$ ;  $R_1=100$   $\Omega$ ;  $R_{gs}=3$  k $\Omega$ ;  $R_{variable}=0$  to 20 k $\Omega$ ; sample  $R\sim 50$   $\Omega$ ;  $R_{monitor}=10$   $\Omega$ ; and Current levels  $\sim 130$  mA. (b) Schematic of tip to sample biasing scheme. T0 represents duration of each voltage step; T1 represents STS data-acquisition time window and T2 represents duration of pulsed injection current. Current duty cycle is ratio of  $\sim T_2/T_0$ .

are  $\sim 4$  ms in duration, and the data-acquisition time window (T1) is  $\sim 40$   $\mu$ s. The injection pulses (T2) are  $\sim 200$   $\mu$ s in duration, both triggered by the voltage steps and synchronized with the data acquisition to cover T1. Transient effects in the measured signal are avoided by rounding the injection-pulse edges. This timing scheme enabled injection duty cycles (ratio of T2 to T0) as low as  $\sim 5\%$ , sufficient to avoid Joule heating<sup>8</sup> in our spin-injection samples.

To demonstrate our STS technique, we have applied it on spin-injection heterostructures comprising thin films of the high- $T_c$  superconductor  $YBa_2Cu_3O_{7-\delta}$  (YBCO) and the half-metallic ferromagnet  $La_{0.7}Ca_{0.3}MnO_3$  (LCMO). Figure 1(a) is a diagram illustrating this injection and measurement processes. The ferromagnetic layer on the left-hand side in Fig. 1(a) provides a source of nearly 100% spin-polarized quasiparticles, which are injected into the middle superconducting layer. The STS setup on the right-hand side of Fig. 1(a) is then used to measure the quasiparticle spectrum of the YBCO, thus directly probing the effects of the spin injection on the high- $T_c$  order parameter.

Figure 1(b) is a schematic of our experimental setup, which shows the STS circuit described earlier combined with our spin-injection heterostructure. The pulsed currents, rendered spin polarized via the LCMO layer, are injected from below and their effect on the top YBCO layer is measured from above. These heterostructures are a trilayer variation of the bilayer structures used in a prior STS study.<sup>9</sup> This trilayer geometry [Fig. 1(b)] was designed to promote uniform injection into the top YBCO layer. In traveling from the bottom YBCO through the LCMO to the top YBCO, the injection current tends to take the path of least resistance. The bottom YBCO layer serves as an equipotential electrode to make all injection paths equally favorable, thus avoiding the so-called transfer-length limitations.<sup>6</sup> For the STS measurement, the tip was kept toward the far side of the injection-current drain (top right-hand side). This was intended to minimize any spectral contribution from “horizontal” pair currents, which could result from quasiparticle recombination after spin relaxation of the injected quasiparticles. The effects of such pair currents are directly investigated in a separate work.<sup>10</sup>

Our spin-injection heterostructures were grown with  $\langle 001 \rangle$  orientation on  $\langle 100 \rangle$  SrTiO<sub>3</sub> (STO) substrates using pulsed laser-ablated deposition and shadow-masking techniques. Epitaxiality between the layers serves to minimize interfacial scattering that could randomize the spin polarization. The YBCO/LCMO/YBCO trilayers are 50 nm/75 nm/50 nm in thickness, with  $\sim 5$  nm STO separating the layers and serving as tunnel barriers. The top YBCO layer is deliberately made thin to minimize spin-diffusion limitations.<sup>6</sup> Typical sample dimensions were  $1 \times 1$  mm<sup>2</sup> for the top YBCO,  $2 \times 1$  mm<sup>2</sup> for the LCMO, and  $4 \times 1$  mm<sup>2</sup> for the bottom YBCO. Details on the sample fabrication procedure, as well as structural characterizations, are given elsewhere.<sup>11</sup>

Our STS measurements were made at 4.2 K, substantially below both the Curie temperature ( $T_m \sim 220$  K) of the LCMO layer and the critical temperature ( $T_c \sim 87$  K) of the YBCO layers. The in-plane critical-current density of the YBCO layers were measured to be  $\sim 3 \times 10^5$  A/cm<sup>2</sup> at 4.2 K, using a similar pulsed transport setup.<sup>12</sup>

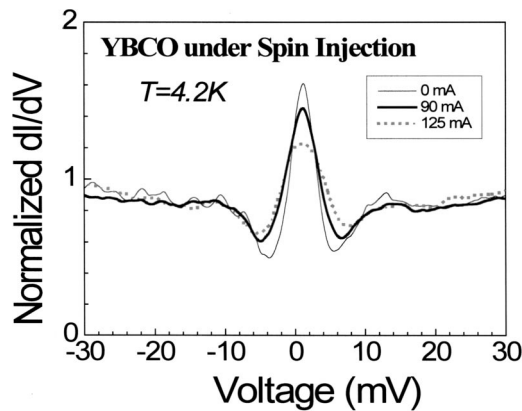


FIG. 3. Normalized conductance ( $dI/dV$ ) curves obtained on YBCO/LCMO/YBCO heterostructures as a function of increasing spin injection. Curves show the evolution of the Andreev-bound states manifested as a ZBCP under spin perturbation. Measurements were performed on near optimally doped YBCO ( $T_c \sim 87$  K) at 4.2 K.

The tunneling conductance spectra,  $dI/dV$ , we measured are similar to those observed in previous studies.<sup>5,9</sup> In this study, we focus on the zero-bias conductance peak (ZBCP), which is a manifestation of the Andreev-bound surface states resulting from the predominant  $d$ -wave pairing symmetry.<sup>13,14</sup> Because Andreev reflection directly involves the creation of a pair,<sup>15</sup> spectral evolution of the ZBCP would reveal how the high- $T_c$  order parameter is affected by the spin injection.

Figure 3 shows the typical evolution of the ZBCP under spin injection at 4.2 K. For clarity, the data have been normalized with respect to the spectral background. The height of the ZBCP is monotonically suppressed with increasing injection current. Accompanying the decrease in the ZBCP height is a slight increase in the ZBCP width. No splitting of the ZBCP was observed, up to the maximum injection level (125 mA) that our pulsed injection circuit could reliably achieve. Assuming the injected quasiparticles are highly spin polarized, this nonsplitting would suggest the  $d$ -wave pairing symmetry is preserved. These results are qualitatively consistent with those seen in our previous work, which used a more rudimentary bilayer heterostructure and a dc-injection circuit. It is important to note that ZBCP splitting would indicate broken time-reversal symmetry (BTRS), which has been reported by planar-junction tunneling done on variously doped YBCO in magnetic fields.<sup>16,17</sup> We see no evidence of such BTRS in our STS experiments, on our near optimally doped YBCO films at 4.2 K, either with or without spin injection.

Our STS data indicate that the energy distribution of

Andreev-bound states in YBCO is altered by quasiparticle spin injection. Since the Andreev-bound states involve pair creation, this spectral redistribution could be interpreted as a signature of dynamic magnetic pair breaking, which introduces finite pair lifetime to produce the observed ZBCP broadening.<sup>18</sup> In this pair-breaking scenario,<sup>19</sup> the spectral broadening provides a measure of the spin-flip Zeeman energy ( $\sim 3$  meV, in our experiment, equivalent to an  $\sim 30$  T exchange field) associated with the itinerant moment due to the injected spins. Further “spin-injection” STS studies would be needed to elucidate these issues, by varying the doping, temperature, and further increasing the injection level using our pulsed-injection technique. Such studies could provide important clues on the high- $T_c$  pairing mechanism, and offer a fundamental understanding of the interplay between itinerant spins and electron pairing. In principle, this technique could also be applied to any material that is amenable to spin injection and heteroepitaxial structuring, as a general method for probing *local* electronic properties under a *bulk* spin perturbation.

This work was supported by grants from NSERC, CFI, OIT, ORDCF, MMO, the Connaught Foundation, and the Canadian Institute for Advanced Research under the Quantum Materials and Nanoelectronics Programs.

- <sup>1</sup>S. H. Pan, E. W. Hudson, K. M. Lang, H. Eisaki, S. Uchida, and J. C. Davis, *Nature* (London) **403**, 746 (2000).
- <sup>2</sup>C. Renner, G. Aeppli, B.-G. Kim, Y.-A. Soh, and S.-W. Cheong, *Nature* (London) **416**, 518 (2002).
- <sup>3</sup>I. Zutic, J. Fabian, and S. Das Sarma, *Rev. Mod. Phys.* (to be published).
- <sup>4</sup>V. A. V'asko, V. A. Larkin, P. A. Kraus, K. R. Nikolaev, D. E. Grupp, C. A. Nordman, and A. M. Goldman, *Phys. Rev. Lett.* **78**, 1134 (1997).
- <sup>5</sup>J. Y. T. Wei, *J. Low Temp. Phys.* **131**, 493 (2003).
- <sup>6</sup>Y. Gim, A. W. Kleinsasser, and J. B. Barner, *J. Appl. Phys.* **90**, 4063 (2001).
- <sup>7</sup>G. Binnig, H. Rohrer, Ch. Gerber, and E. Weibel, *Appl. Phys. Lett.* **40**, 178 (1982).
- <sup>8</sup>P. Mikheenko, M. S. Colclough, C. Severac, R. Chakalov, F. Welhoffer, and C. M. Muirhead, *Appl. Phys. Lett.* **78**, 356 (2001).
- <sup>9</sup>J. Y. T. Wei, N.-C. Yeh, C. C. Fu, and R. P. Vasquez, *J. Appl. Phys.* **85**, 8 (1999).
- <sup>10</sup>J. Ngai, P. Morales, and J. Y. T. Wei (unpublished).
- <sup>11</sup>J. Ngai, M.Sc. thesis, University of Toronto, 2002.
- <sup>12</sup>P. Morales, M.Sc. thesis, University of Toronto, 2003.
- <sup>13</sup>C.-R. Hu, *Phys. Rev. Lett.* **72**, 1526 (1994).
- <sup>14</sup>Y. Tanaka and S. Kashiwaya, *Phys. Rev. Lett.* **74**, 3451 (1995).
- <sup>15</sup>J. Y. T. Wei, N.-C. Yeh, D. F. Garrigus, and M. Strasik, *Phys. Rev. Lett.* **81**, 2542 (1998).
- <sup>16</sup>M. Aprili, E. Badica, and L. H. Greene, *Phys. Rev. Lett.* **83**, 4630 (1999).
- <sup>17</sup>Y. Dagan and G. Deutscher, *Phys. Rev. Lett.* **87**, 177004 (2001).
- <sup>18</sup>S. Skalski, O. Betbeder-Matibet, and P. R. Weiss, *Phys. Rev.* **136**, A1500 (1964).
- <sup>19</sup>A. G. Aronov, *JETP Lett.* **24**, 32 (1976); *Sov. Phys. JETP* **44**, 193 (1976).